Laser and Particle Beams (2012), *30*, 613–619.

doi:10.1017/S0263034612000699

Experimental verification of a low-impedance transit-time oscillator without foils

YIBING CAO, JUNTAO HE, JIANDE ZHANG, AND JUNPU LING

College of Optoelectronic Science and Engineering, National University of Defense Technology, Changsha, People's Republic of China

(RECEIVED 28 June 2012; ACCEPTED 1 August 2012)

Abstract

The low-impedance transit-time oscillator without foils is a new high-power microwave generator. In a previous report, a radiation power of 2.7 GW at 1.64 GHz has been achieved and the corresponding power conversion efficiency is 18.75%. Recently, the further experiments are continued in our laboratory. By increasing the cathode-anode gap properly, the operating voltage of device is enhanced to about 628 kV, and the corresponding radiation power reaches 3.6 GW. The device efficiency approaches 23%. In the newest experiments, because of the higher power level, the radiation power has been obviously influenced by RF breakdown in the vicinity of the dielectric window. By using a plastic bag filled with sulfur-hexafluoride (SF_6), such an influence can be minimized.

Keywords: High power microwave; Low-impedance; RF breakdown; Transit-time

1. INTRODUCTION

Although many new directions are becoming more and more attractive in the high-power microwave (HPM) domain (Fan *et al.*, 2007; Ge *et al.*, 2010; He *et al.*, 2011; Korovin *et al.*, 2003; Li *et al.*, 2010; Zhang *et al.*, 2010), advancing the peak power is always one of the most important considerations. Effective methods are to increase the input electric power or enhance the device efficiency. In pursuit of high power conversion efficiency, many efforts have been done and significant progress has been achieved (Barker *et al.*, 2001; Shkvarunets *et al.*, 2002; Teng *et al.*, 2009; Xiao *et al.*, 2009, 2010, 2011). The highest power so far was obtained by the multiwave Cerenkov generator and relativistic klystron amplifier in the 1990s (Bugaev *et al.*, 1990; Serlin *et al.*, 1994). The corresponding efficiencies are respectively 50% and 40%. However, it seems to be very difficult for the HPM devices to further enhance the power conversion efficiency with the exception of the sources based on super radiance (Anton *et al.*, 2003; Bandurkin *et al.*, 2011).

In order to obtain higher output microwave power, increasing the input electric power may be a more feasible method (Arman, 1996; Cao *et al.*, 2009; He *et al.*, 2004; Yang *et al.*, 2005). With the fast development of pulsed power technology, an intense relativistic electron beam (IREB) over 20 GW electric powers can be easily provided by many pulsed power sources (Adam *et al.*, 2007; Ouyang *et al.*, 2008; Yatsui *et al.*, 2005; Zhang *et al.*, 2007; Zou *et al.*, 2006). Even if the efficiency of HPM devices is only 10%, a microwave power of 2.0 GW can still be obtained. However, most HPM devices so far operate at a high diode impedance (about 100 Ω) (Fan *et al.*, 2004; Hahn *et al.*, 2002; Levine *et al.*, 1994; Zhang *et al.*, 2004, 2011), which is disadvantageous to match with the low-impedance pulsed power sources providing high electric power (about 20 Ω) (Liu *et al.*, 2006, 2007*a*, 2007*b*, 2009; Zou *et al.*, 2006). This has greatly limited further improvement of the microwave power.

In our previous work, a low-impedance transit-time oscillator without foils (LITTO) has been put forward (Cao *et al.*, 2009). The device impedance is about 20 Ω and can thus utilize ultrahigh-current electron beams to reach high peak power. With a 600 kV, 24 kA electron beam guided by an external magnetic field of 0.5 Tesla, a radiation power of 2.7 GW at 1.64 GHz has been achieved in the experiments (Cao *et al.*, 2012). Recently, the further experiments are continued in our laboratory. This article briefly introduces the newest experimental results.

2. EXPERIMENTAL IMPROVEMENT

According to the particle-in-cell (PIC) simulation (Cao *et al.*, 2009), the power conversion efficiency peaks at about

Address correspondence and reprint requests to: Juntao He, College of Optoelectronic Science and Engineering, National University of Defense Technology, Changsha 410073, People's Republic of China.
E-mail: hjt0731@163.com

700 kV, which is treated as the optimal working voltage of the LITTO. Operating at the optimal voltage, the highly modulated electron beam can deliver more possible power to the radio frequency (RF) field because of perfect synchronism between the electron transit time and the RF period. However, in previous experiments, the operating voltage of the LITTO is basically lower than 600 kV. We failed in all our attempts to further increase the diode voltage.

From previous experimental results (Cao *et al.*, 2012), it is found that the saturated diode voltage gradually decreases with the increasing time and the beam current is just the reverse. Figure 1 shows the variations of the voltage and current versus time. Maybe the varying diode impedance is responsible for these. With the expansion of the cathode plasma (Roy *et al.*, 2009), the cathode-anode gap is gradually decreased and thus lowering the corresponding diode impedance (see Fig. 2). Supposing the electric power provided by the accelerator is stabilized at P, the diode voltage V and the beam current I can be respectively expressed as

$$\begin{aligned} V &= \sqrt{PR} \\ I &= \sqrt{P/R} \end{aligned}, \tag{1}$$

where R is the diode impedance. Therefore, it is inevitable that the voltage and the current will, respectively, decrease and increase because of the lowering diode impedance (see Fig. 2). In the newest experiments, we tried to slightly enhance the impedance by enlarging the cathode-anode gap from previous 15 mm to 20 mm. Eventually, the average operating voltage is indeed increased to about 630 kV.

3. EXPERIMENTAL RESULTS

Figure 3 illustrates our overall experimental arrangement. The operating voltage provided by the IREB accelerator can be varied by changing the trigger time of the main switch. The measures of the voltage, current and microwave

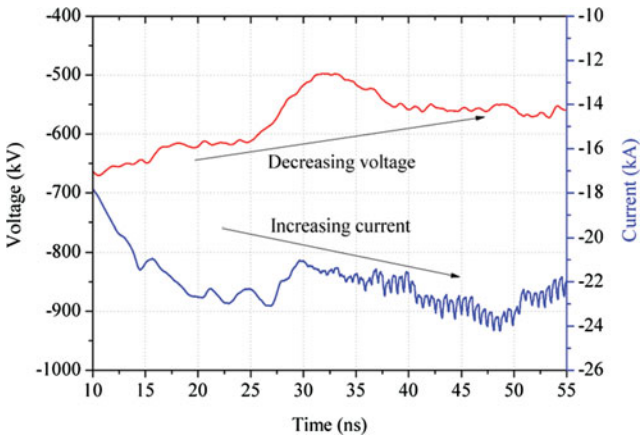

Fig. 1. (Color online) Variations of diode voltage and current versus time.

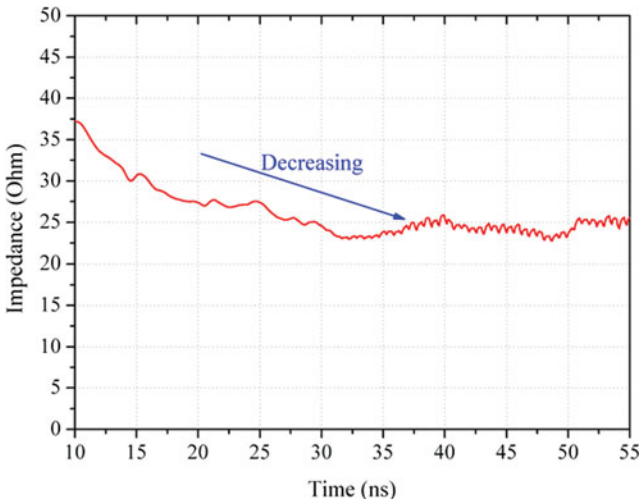

Fig. 2. (Color online) Variation of diode impedance versus time.

have been introduced in detail in our previous paper (Cao *et al.*, 2012). The directional couplers and the microwave crystal detectors are also the same with those used there. In the newest experiments, the signals from the directional couplers are, respectively, attenuated 37.87 dB and 43.90 dB before passing through the crystal detectors.

In order to identify the operating mode in the new state, the microwave frequency is first measured in the experiments. Figure 4 gives the relationship between the diode voltage and the operating frequency. From the figure, it can be seen that the microwave frequency varies between 1.63 GHz and 1.64 GHz with the changed voltage. After voltage is beyond 530 kV, the microwave frequency is stabilized at 1.639 GHz, which agrees well with the simulation result. With an input electron beam of 553 kV voltage and 21 kA current guided by an external magnetic field of 0.5 Tesla, the experimental radiation pattern is shown in Figure 5, which is basically consistent with the numerical result, indicating that the radiation mode is TM_{01}. Typical experimental waveforms of the diode voltage, diode current, and two output microwave signals measured in the far-field are shown in Figure 6. The integrated power was 2.45 GW,

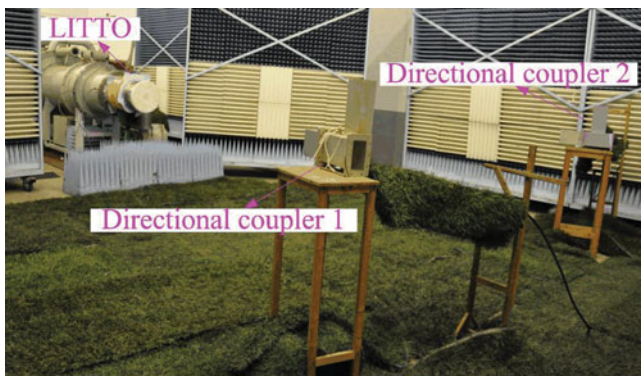

Fig. 3. (Color online) Photograph of the experimental layout.

https://doi.org/10.1017/S0263034612000699 Published online by Cambridge University Press

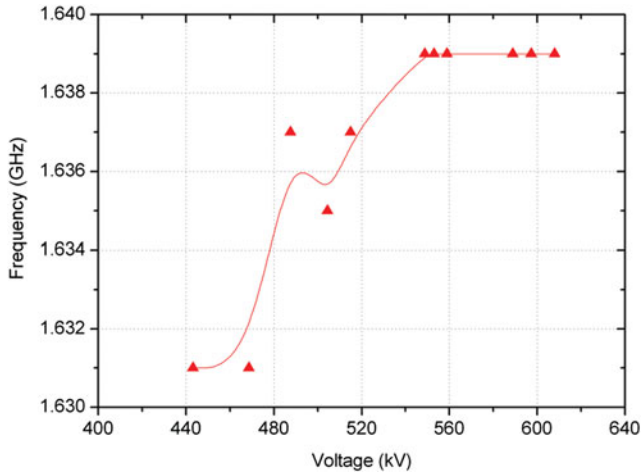

Fig. 4. (Color online) Microwave frequency versus diode voltage.

which is slightly lower than the simulation result (about 2.6 GW). The corresponding pulse width was about 32 ns, close to that obtained by the PIC simulation, indicating that there was no obvious pulse shortening.

According to the PIC simulation (Cao *et al.*, 2009), the microwave power should gradually increase with the increasing diode voltage and the power conversion efficiency peaks at about 700 kV. However, when the experimental voltage is increased up to 628 kV (the corresponding current is 25 kA), the radiated microwave power has not increased obviously. The corresponding waveforms of the diode voltage, diode current, and two output microwave signals measured in the far-field are shown in Figure 7. The evaluated microwave power was 2.40 GW, with an efficiency of only 15.5%. Several shots showed similar results. With the similar voltage and current, a 3.7 GW microwave has been obtained in the simulation. In order to draw a comparison, the microwave powers of the experiment and simulation are shown in Figure 8. Obviously, the experimental power is much lower

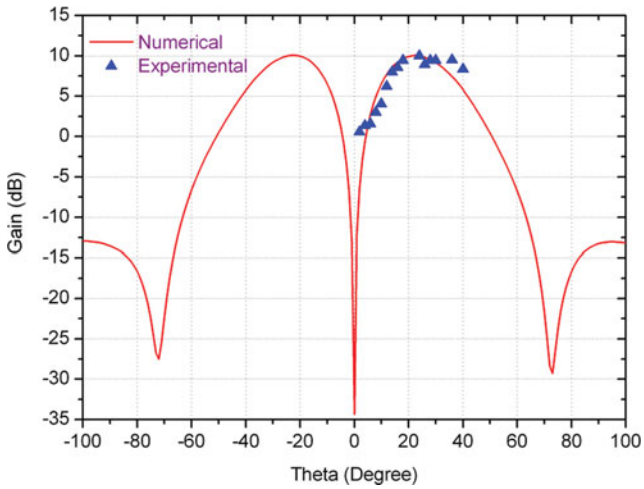

Fig. 5. (Color online) Radiation pattern of the system.

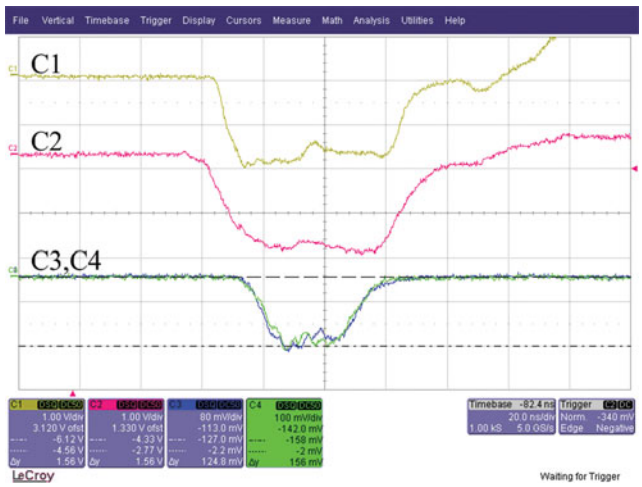

Fig. 6. (Color online) Waveforms of the diode voltage (C1), diode current (C2), microwave detector signals (C3, C4) (diode voltage 553 kV, diode current 21 kA, microwave power 2.45 GW, 20 ns/div).

than the simulation result. One probable explanation is that the RF breakdown in the vicinity of the dielectric window has limited the radiation of HPM.

In previous experiments, the RF breakdown has been observed. Fortunately, the RF breakdown there didn't obviously influence the microwave radiation and the breakdown phenomenon was only used to judge the operating modes (He *et al.*, 2012). Nevertheless, with the improved radiation power, the rapidly increasing plasma caused by the RF breakdown could reflect a fraction of HPM radiation. As shown in Figure 9, the light caused by the RF breakdown is obviously much more intense than those in previous experiments.

The electric field intensity on the interface between dielectric and air is first analyzed by numerical calculation. With a 3.5 GW input at 1.64 GHz, Figure 10 gives the electric field

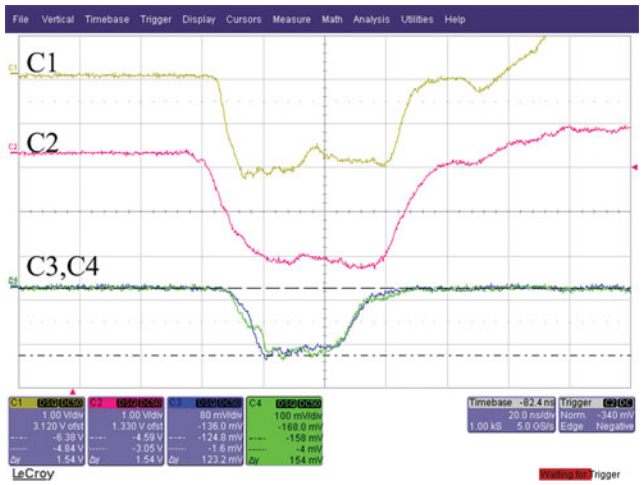

Fig. 7. (Color online) Waveforms of the diode voltage (C1), diode current (C2), microwave detector signals (C3, C4) (diode voltage 628 kV, diode current 25 kA, microwave power 2.40 GW, 20 ns/div).

https://doi.org/10.1017/S0263034612000699 Published online by Cambridge University Press

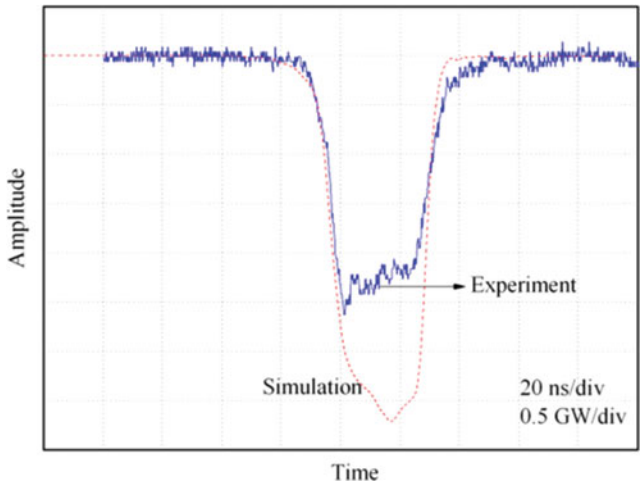

Fig. 8. (Color online) Microwave output powers from the simulation and experiment.

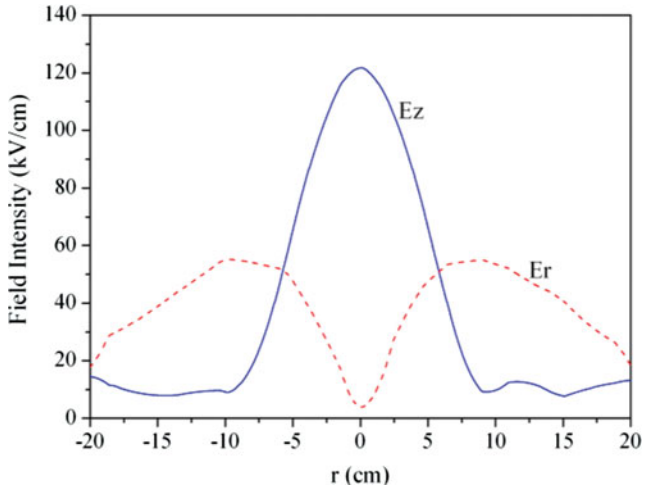

Fig. 10. (Color online) Electric field components versus radius r.

variation along the radial position on the interface, corresponding to the TM_{01} mode radiation. As shown in the figure, the maximum axial electric field is about 120 kV/cm and the maximum radial electric field approaches 60 kV/cm. Both of them are greatly beyond the air breakdown threshold (20–30 kV/cm) (Booske, 2008). Therefore, it is very probable that fierce RF breakdown would happen in the vicinity of window. Figure 11 displays the electric field distributions on the interface. From this figure, it can be concluded that the RF breakdown caused by the axial and radial field components would happen at different position. In combination with Figure 10, it can be concluded that the present breakdown is mainly caused by the axial field components.

After using a clear plastic bag filled with SF_6, the RF breakdown is effectively suppressed and the corresponding result is shown in Figure 12. Although a trifling surface flashover caused by the radial field still exists (corresponding to Fig. 11b), it hardly affects the radiated microwave and the integrated power is increased from 2.5 GW to 3.6 GW, which agrees well with the simulation results (about 3.7 GW). Figure 13 gives the typical experimental waveforms of the diode voltage, diode current, and two output microwave signals measured in the experiments. Several shots showed similar results. After taking off the clear plastic bag filled with SF_6, the microwave power measured in the far-field is again decreased to about 2.5 GW and the corresponding RF breakdown as shown in Figure 9 is still observed.

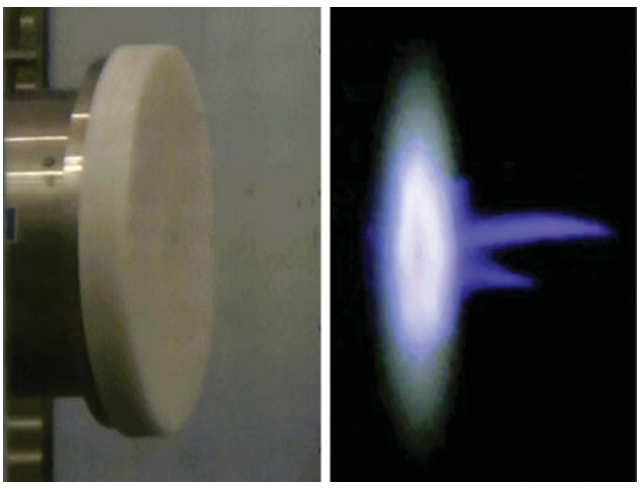

Fig. 9. (Color online) Photographs of window RF breakdown in the atmosphere.

4. DISCUSSIONS

High input electric power and output microwave power is treated as a main merit of the LITTO, which has been testified by the simulation and experimental results. Dielectric window breakdown is demonstrated to be a major issue in the transmission of HPM radiation (Krile *et al.*, 2006; Kuo *et al.*, 1990, 1991; Liu *et al.*, 2000; Nam *et al.*, 2009; Woo *et al.*, 1984). Plasma caused by RF breakdown will bring some negative impacts on the HPM, such as reflection, absorption attenuation, and so on. Consequently, the measured microwave power in the experiments is obviously decreased. In order to depress RF breakdown, a clear plastic bag filled with SF_6 has been used and the microwave power is significantly increased.

However, further investigation is limited by the available voltage level and its pulse width. In fact, it is not obvious to enhance the diode voltage by enlarging the cathode-anode gap. The present voltage is still less than 700 kV. Besides, due to the limited pulse width, it may be difficult for the plasma to build up to the extent that it cuts-off the radiated microwave. Along with an increasing voltage pulse width, the influence from space-time-dependent plasma would probably get more and more significant.

The LITTO is also expected long-pulsed and repetitive operation. Although no obvious pulse shortening is observed

https://doi.org/10.1017/S0263034612000699 Published online by Cambridge University Press

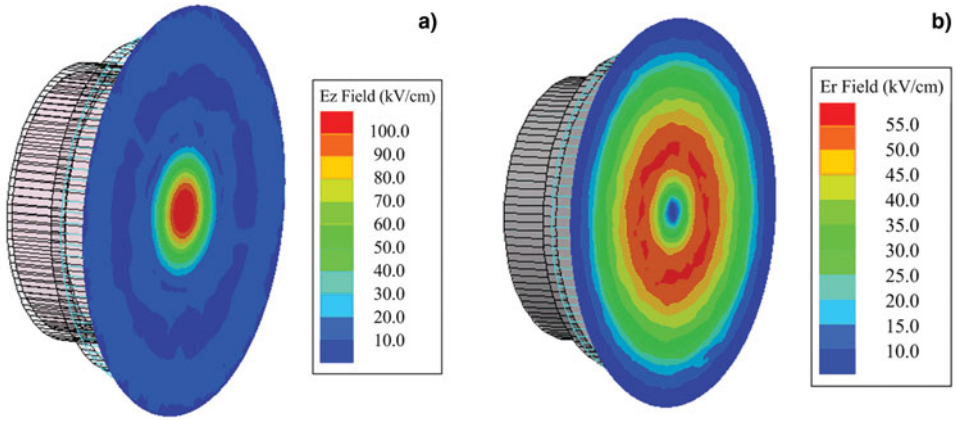

Fig. 11. (Color online) Distributions of axial electric field (**a**) and radial electric field (**b**) on the dielectric-air interface.

Fig. 12. (Color online) Photographs of window RF breakdown in the atmosphere with a clear plastic bag filled with SF_6.

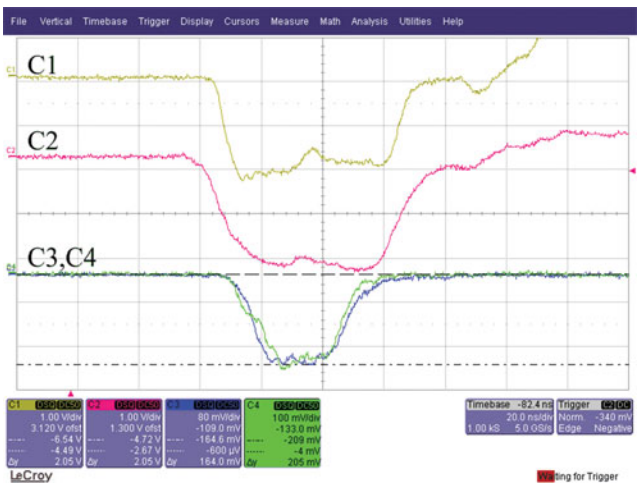

Fig. 13. (Color online) Waveforms of the diode voltage (C1), diode current (C2), microwave detector signals (C3, C4) (diode voltage 628 kV, diode current 25 kA, microwave power 3.6 GW, 20 ns/div).

in the present experiment, the ability of long-pulsed and repetitive operation is still indistinct because of the limited voltage pulse width. A fatal shortcoming is the design of the electron collector, which has been greatly neglected in previous investigation (Cao *et al.*, 2009). Experiment indicated that the material of the electron collector has great influence on the generation of HPM (He *et al.*, 2012). When the collector is stainless steel, intense electrons reflection and plasma formation on the collector would result in high-order mode excitation and pulse shortening. The mode competition has been effectively depressed by using a graphite collector instead of the stainless steel collector. However, as the voltage pulse width increases, the dust from the IREB impact on the graphite collector also probably contaminates the device and results in pulse shortening.

5. CONCLUSIONS

The LITTO is a new low-impedance HPM source. A simple structure makes such a device attractive. Simultaneously, due to a short length (about 50 cm), it is very advantageous to the transportation of IREB (Konoplev *et al.*, 2006). The experiments have demonstrated that such a device can allow high input and output powers. With an IREB of 628 kV voltage and 25 kA current, guiding by a magnetic field of 0.5 Tesla, a 3.6 GW radiated microwave at frequency 1.639 GHz has been obtained in the experiments. The device efficiency approaches 23%. The experimental results agree well with those of simulation. No obvious pulse shortening phenomenon has been observed in the present experiment. The intensive investigation will be continued on a long-pulsed IREB generator.

ACKNOWLEDGMENT

This work was supported by the National Natural Science Foundation of China under Grant No. 61171021.

REFERENCES

Adam, L., Anders, L., Hans, B. & Mats, L. (2007). 45 GW pulsed-power generator. *16th IEEE International Pulsed Power Conference*, 1272–1275.

Anton, A.E., Sergei, D.K., Vladislav, V.R., Igor, V.P., Gennady, A.M., Sergei, N.R., Valery, G.S., Michael, I.Y. & Naum, S.G.

https://doi.org/10.1017/S0263034612000699 Published online by Cambridge University Press

(2003). Production of short microwave pulses with a peak power exceeding the driving electron beam power. *Laser Part. Beams* **21**, 187–196.

Arman, M.J. (1996). Radial acceletron, a new low-impedance HPM source. *IEEE Trans. Plasma Sci*. **24**, 964–969.

Bandurkin, I.V. & Savilov, A.V. (2011). Super-radiant Cherenkov backward-wave oscillator with cyclotron absorption. *Appl. Phys. Lett*. **99**, 193506.

Barker, R.J. & Schamiloglu, E. (2001). *High-Power Microwave Sources and Technologies*. New York: IEEE.

Booske, J.H. (2008). Plasma physics and related challenges of millimeter-wave-to-terahertz and high power microwave generation. *Phys. Plasmas* **15**, 055502.

Bugaev, S.P., Cherepenin, V.A., Kanavets, V.I., Klimov, A.I., Kopenkin, A.D., Koshelev, V.I., Popov, V.A. & Slepkov, A.I. (1990). Relativistic multiwave cerenkov generators. *IEEE Trans. Plasma Sci*. **18**, 525–536.

Cao, Y.B., Zhang, J.D. & He, J.T. (2009). A low-impedance transit-time oscillator without foils. *Phys. Plasmas* **16**, 083102.

Cao, Y.B., He, J.T. & Zhang, J.D. (2012). High power microwave generation from the low-impedance transit-time oscillator without foils. *Phys. Plasmas* **19**, 072106.

Fan, Y.W., Zhong, H.H., Li, Z.Q., Shu, T., Zhang, J.D., Zhang, J., Zhang, X.P., Yang, J.H. & Luo, L. (2007). A double-band high-power microwave source. *J. Appl. Phys*. **102**, 103304.

Fan, Z., Liu, Q., Chen, D., Tan, J. & Zhou, H. (2004). Theoretical and experimental researches on C-band three-cavity transit-time effect oscillator. *Sci. China Ser. G* **47**, 310–329.

Ge, X.J., Zhong, H.H., Qian, B.L., Zhang, J., Gao, L., Jin, Z.X., Fan, Y.W. & Yang, J.H. (2010). An L-band coaxial relativistic backward wave oscillator with mechanical frequency tunability. *Appl. Phys. Lett*. **97**, 101503.

Hahn, K., Fuks, M.I. & Schamiloglu, E. (2002). Initial studies of a long-pulse relativistic backward-wave oscillator utilizing a disk cathode. *IEEE Trans. Plasma Sci*. **30**, 1112–1119.

He, J.T., Cao, Y.B., Zhang, J.D. & Ling, J.P. (2012). Effects of intense relativistic electron beam on the microwave generation in a foil-less low-impedance transit-time oscillator. *IEEE Trans. Plasma Sci*. **40**, 1622–1631.

He, J.T., Cao, Y.B., Zhang, J.D., Wang, T. & Ling, J.P. (2011). Design of a dual-frequency high-power microwave generator. *Laser Part. Beams* **29**, 479–485.

He, J.T., Zhong, H.H. & Liu, Y.G. (2004). A new low-impedance high power microwave source. *Chin. Phys. Lett*. **21**, 1111–1113.

Konoplev, I.V., Cross, A.W., MacInnes, P., He, W., Whyte, C.G., Phelps, A.D.R., Robertson, C.W., Ronald, K. & Young, A.R. (2006). High-current oversized annular electron beam formation for high-power microwave research. *Appl. Phys. Lett*. **89**, 171503.

Korovin, S.D., Kurkan, I.K., Loginov, S.V., Pegel, I.V., Polevin, S.D., Volkov, S.N. & Zherlitsyn, A.A. (2003). Decimeter-band frequency-tunable sources of high-power microwave pulses. *Laser Part. Beams* **21**, 175–185.

Krile, J.T., Neuber, A.A., Krompholz, H.G. & Gibson, T.L. (2006). Monte Carlo simulation of high power microwave window breakdown at atmospheric conditions. *Appl. Phys. Lett*. **89**, 201501.

Kuo, S.P. & Zhang, Y.S. (1991). A theoretical model for intense microwave pulse propagation in an air breakdown environment. *Phys. Fluids B* **3**, 2906–2912.

Kuo, S.P., Zhang, Y.S. & Kossey, P. (1990). Propagation of high power microwave pulses in air breakdown environment. *J. Appl. Phys*. **67**, 2762–2766.

Levine, J.S. & Harteneck, B.D. (1994). Repetitively pulsed relativistic klystron amplifier. *Appl. Phys. Lett*. **65**, 2133–2135.

Li, G.L., Shu, T., Yuan, C.W., Zhu, J., Liu, J., Wang, B. & Zhang, J. (2010). Simultaneous operation of X band gigawatt level high power microwaves. *Laser Part. Beams* **28**, 35–44.

Liu, G.Z., Liu, J.Y., Huang, W.H., Zhou, J.S., Song, X.X. & Ning, H. (2000). A study of high power microwave air breakdown. *Chin. Phys*. **9**, 757–763.

Liu, J.L., Cheng, X.B., Qian, B.L., Ge, B., Zhang, J.D. & Wang, X.X. (2009). Study on strip spiral Blumlein line for the pulsed forming line of intense electron-beam accelerators. *Laser Part. Beams* **27**, 95–102.

Liu, J.L., Li, C.L., Zhang, J.D., Li, S.Z. & Wang, X.X. (2006). A spiral strip transformer type electron-beam accelerator. *Laser Part. Beams* **24**, 355–358.

Liu, J.L., Yin, Y., Ge, B., Zhan, T.W., Cheng, X.B., Feng, J.H., Shu, T., Zhang, J.D. & Wang, X.X. (2007*a*). An electron-beam accelerator based on spiral water PFL. *Laser Part. Beams* **25**, 593–599.

Liu, J.L., Zhan, T.W., Zhang, J., Liu, Z.X., Feng, J.H., Shu, T., Zhang, J.D. & Wang, X.X. (2007*b*). A Tesla pulse transformer for spiral water pulse forming line charging. *Laser Part. Beams* **25**, 305–312.

Nam, S.K., Lim, C. & Verboncoeur, J.P. (2009). Dielectric window breakdown in oxygen gas: Global model and particle-in-cell approach. *Phys. Plasmas* **16**, 023501.

Ouyang, J., Liu, Y.G., Liu, J.L., Wang, M.X. & Feng, J.H. (2008). Research on a Folded Blumlein Line Using Kapton Film as Dielectrics. *Plasma Sci. Technol*. **10**, 231–234.

Roy, A., Menon, R., Mitra, S., Kumar, S., Sharma, V. & Nagesh, K.V. (2009). Plasma expansion and fast gap closure in a high power electron beam diode. *Phys. Plasmas* **16**, 053103.

Serlin, V. & Friedman, M. (1994). Development and optimization of the RKA. *IEEE Trans. Plasma Sci*. **22**, 692–700.

Shkvarunets, A.G., Carmel, Y., Nusinovich, G.S., Abu-elfadl, T.M., Rodgers, J., Antonsen Jr., T.M., & Granatstein, V. (2002). Realization of high efficiency in a plasma-assisted microwave source with two-dimensional electron motion. *Phys. Plasmas* **9**, 4114–4117.

Teng, Y., Liu, G., Shao, H. & Tang, C. (2009). A new reflector designed for efficiency enhancement of CRBWO. *IEEE Trans. Plasma Sci*. **37**, 1062–1068.

Woo, W. & Degroot, J.S. (1984). Microwave absorption and plasma heating due to microwave breakdown in the atmosphere. *Phys. Fluids* **27**, 475–487.

Xiao, R.Z., Chen, C.H., Sun, J., Zhang, X.W & Zhang, L.J. (2011). A high-power high-efficiency klystron-like relativistic backward wave oscillator with a dual-cavity extractor. *Appl. Phys. Lett*. **98**, 101502.

Xiao, R.Z., Chen, C.H., Zhang, X.W. & Sun, J. (2009). Efficiency enhancement of a high power microwave generator based on a relativistic backward wave oscillator with a resonant reflector. *J. Appl. Phys*. **105**, 053306.

Xiao, R.Z., Zhang, X.W., Zhang, L.J., Li, X.Z., Zhang, L.G., Song, W., Hu, Y.M., Sun, J., Huo, S.F., Chen, C.H., Zhang, Q.Y. & Liu, G.Z. (2010). Efficient generation of multi-gigawatt

power by a klystron-like relativistic backward wave oscillator. *Laser Part. Beams* **28**, 505–511.

Yang, W. & Ding, W. (2005). Studies of a low-impedance coaxial split-cavity oscillator. *Phys. Plasmas* **12**, 063105.

Yatsui, K., Shimiya, K., Masugata, K., Shigeta, M. & Shibata, K. (2005). Characteristics of pulsed power generator by versatile inductive voltage adder. *Laser Part. Beams* **23**, 573–581.

Zhang, J., Jin, Z.X., Yang, J.H., Zhong, H.H., Shu, T., Zhang, J.D., Qian, B.L., Yuan, C.W., Li, Z.Q., Fan, Y.W., Zhou, S.Y. & Xu, L.R. (2011). Recent advance in long-pulse HPM sources with repetitive operation in S-, C-, and X-bands. *IEEE Trans. Plasma Sci*. **39**, 1438–1445.

Zhang, J., Zhong, H.H. & Luo, L. (2004). A novel overmoded slow-wave high-power microwave (HPM) generator. *IEEE Trans. Plasma Sci*. **32**, 2236–2242.

Zhang, Q., Yuan, C.W. & Liu, L. (2010). Design of a dual-band power combining architecture for high-power microwave applications. *Laser Part. Beams* **28**, 377–385.

Zhang, Y.H., Chang, A.B., Xiang, F., Song, F.L., Kang, Q., Luo, M., Li, M.J. & Gong, S.G. (2007). Repetition rate of intense current electron-beam diodes using 20 GW pulsed source. *Acta Phys. Sin*. **56**, 5754–5757.

Zou, X.B., Liu, R., Zeng, N.G., Han, M., Yuan, J.Q., Wang, X.X. & Zhang, G.X. (2006). A pulsed power generator for x-pinch experiments. *Laser Part. Beams* **24**, 503–509.

https://doi.org/10.1017/S0263034612000699 Published online by Cambridge University Press